ACS APPLIED MATERIALS & INTERFACES

Research Article

www.acsami.org

One-Pot Synthesis of Monodisperse 5 nm Pd–Ni Nanoalloys for Electrocatalytic Ethanol Oxidation

Kyungwon Lee,[†] Shin Wook Kang,[†] Su-Un Lee, Kyu-Hwan Park, Young Wook Lee, and Sang Woo Han*

Department of Chemistry and KI for the NanoCentury, KAIST, Daejeon 305-701, Korea

Supporting Information

ABSTRACT: Highly monodisperse 5 nm Pd–Ni alloy nanoparticles (NPs) were prepared by the reduction of $Pd(acac)_2/Ni(acac)_2$ mixtures with tert-butylamine-borane complex (TBAB) in the presence of oleic acid (OA) and oleylamine (OAm). Employing TBAB as an effective reductant and OA/OAm combination as an effective stabilizing agent is crucial to the formation of monodisperse Pd–Ni NPs. Experimental results collectively verify that the Pd–Ni alloy NPs form through the sequential nucleation-interdiffusion process and the simultaneous reduction of both metal precursors by the one-pot protocol is the key to the formation of homogeneous NPs. The Pd–Ni NPs were well-dispersed on carbon supports and chemically dealloyed after acetic acid washing through the selective dissolution of the less noble Ni component. The Pd–Ni NP catalysts exhibited much higher electrocatalytic activity and stability for ethanol oxidation than those of a commercial Pd/C catalyst.

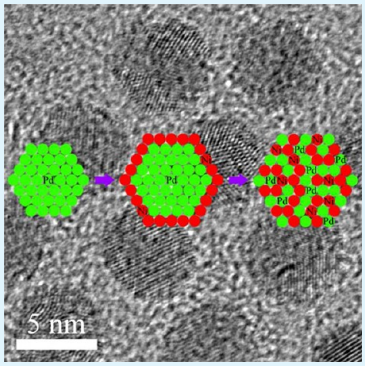

KEYWORDS: *monodisperse nanoparticles, Pd–Ni alloy, ethanol oxidation, fuel cell*

INTRODUCTION

The direct ethanol fuel cell (DEFC) has attracted a great deal of attention because of the high energy density of ethanol and the ease of handling liquid fuel.[1] Moreover, compared to methanol, ethanol has advantages of low toxicity and renewability.[2] However, broad application of DEFCs has been limited because of the high cost and low long-term stability of Pt, which has been commonly used as an efficient catalyst for fuel oxidation.[3] To address the cost and stability issues, Pd-based nanostructures have been extensively explored as alternative electrocatalysts to replace Pt-based catalysts for ethanol oxidation reaction.[4−7] Specifically, alloy nanoparticles (NPs) consisting of Pd and non-noble metals have been considered as the one of the best alternative economical catalysts with desired performance.[4] Indeed, bimetallic alloy NPs usually show improved catalytic functions being distinct from those of the corresponding monometallic counterparts, which can be attributed to the synergistic effect between constituent metals.[8]

Among Pd-non-noble metal NPs, Pd–Ni NPs have been investigated by numerous research groups because of their prominent electrocatalytic activity.[9−14] The production of Pd–Ni NPs has been achieved through various synthetic approaches, such as electrodeposition,[9] radiolysis,[10] and wet chemical methods.[11−14] However, most of the synthesized Pd–Ni NPs have average particle diameters larger than 10 nm and broad size distributions. Hence, development of a facile synthetic strategy for the preparation of sub-10 nm Pd–Ni NPs with controlled composition and uniform shape and size is strongly required to optimize their catalytic performance. Herein, we report a facile and reproducible one-pot synthesis method of monodisperse Pd–Ni alloy NPs with an average size of 5 nm. Pd–Ni NPs were prepared by the simultaneous reduction of $Pd(acac)_2$ (acac = acetylacetonate) and $Ni(acac)_2$ using tert-butylamine-borane complex (TBAB) as a reductant in the presence of oleic acid (OA) as a stabilizer and oleylamine (OAm) as both a solvent, co-reductant, and co-surfactant. The enhanced electrocatalytic activity and stability of carbon-supported Pd–Ni alloy NPs toward ethanol oxidation were also demonstrated in alkaline medium.

EXPERIMENTAL SECTION

Chemicals and Materials. Palladium(II) acetylacetonate ($Pd(acac)_2$, Aldrich, 99%), nickel(II) acetylacetonate ($Ni(acac)_2$, Aldrich, 95%), TBAB (Aldrich, 97%), OA (Aldrich, 90%), OAm (Aldrich, 70%), and commercial Pd/C (Aldrich, 10 wt %) were all used as received. Other chemicals, unless specified, were reagent grade, and triply distilled water with a resistivity of greater than 18.0 MΩ cm was used in the preparation of aqueous solutions.

Preparation of Pd–Ni Alloy NPs. The synthesis was carried out under an airless environment. In a typical synthesis of Pd–Ni alloy NPs, a $Pd(acac)_2/Ni(acac)_2$ mixture in a molar ratio of 1/1 (0.05/0.05 mmol) or 1/3 (0.05/0.15 mmol) and 0.3 or 0.5 mmol of TBAB were dissolved in a mixture of OA (0.2 mL) and OAm (10 mL) at room temperature, and the mixture was stirred for 30 min under an argon flow. Then, the reaction solution was heated to 270 or 290 °C with a constant heating rate of 15 °C min^{-1}, and kept at that temperature for 20 min. The resultant solution was cooled down to room temperature. The final product was washed and separated by centrifugation (10 000 rpm for 10 min), and then dispersed in hexane.

Received: May 23, 2012
Accepted: July 16, 2012
Published: July 16, 2012

Preparation of Pd–Ni NPs/C Catalysts. The 8.5 mg of $Pd_{50}Ni_{50}$ alloy NPs and 33.8 mg of Ketjen Black carbon were mixed with hexane and sonicated for 5 h. In the case of $Pd_{25}Ni_{75}$ NPs, 14.6 mg of $Pd_{25}Ni_{75}$ NPs, and 58.5 mg of Ketjen Black carbon were mixed. After the hexane was evaporated, 20 mL of acetic acid was poured into the catalysts and vigorously stirred at 80 °C for overnight. The reaction mixture was cooled down to room temperature, and the product was washed with ethanol and separated by centrifugation at 10 000 rpm for 20 min. This procedure was repeated at least 5 times. From the inductively coupled plasma-atomic emission spectroscopy (ICP-AES) measurements, the Pd loadings of Pd–Ni NPs/C catalysts prepared from 1:1 and 1:3 molar ratios of $Pd(acac)_2/Ni(acac)_2$ were estimated to be 9.04 and 4.83 wt %, respectively.

Characterization. Transmission electron microscopy (TEM) and high-resolution TEM (HRTEM) characterizations were performed using a Phillips Model Tecnai F20 transmission electron microscope operating at 200 kV after placing a drop of NP solution on carbon-coated Cu grids (200 mesh). High-angle annular dark-field scanning TEM (HAADF-STEM) and energy-dispersive X-ray spectroscopy (EDS) measurements were performed using a JEM-ARM200F spherical aberration corrected scanning transmission electron microscope (Cs-corrected STEM, JEOL) operating at 200 kV. The effective electron probe size used in HAADF-STEM-EDS experiments was 0.2 nm. X-ray diffraction (XRD) patterns were obtained using a Rigaku D/Max-2500 diffractometer with Cu Kα (0.1541 nm) radiation. The compositions of NPs were determined by ICP-AES (Spectro Ciros). X-ray photoelectron spectroscopy (XPS) measurements were carried out using a Thermo VG Scientific Sigma Probe spectrometer with Al Kα X-ray (1486.6 eV) as the light source. Cyclic voltammetry (CV) measurements were carried out in a conventional three-electrode cell using a CH Instrument model 600C potentiostat. Catalysts-loaded glassy carbon electrode (GCE) with a diameter of 3 mm served as a working electrode. The GCE was polished with alumina powder and thoroughly washed with high-purity water before use. Pt wire and Ag/AgCl (in saturated 3 M NaCl) were used as the counter and reference electrodes, respectively. The total loaded amounts of Pd on GCE were adjusted to 28.29 μg cm^{-2} for all samples. Before CV measurements, the catalysts-modified GCEs were covered with diluted 0.05% Nafion solution and dried at room temperature. All CV curves were obtained at room temperature. The electrolyte solutions were purged with high-purity N_2 gas before use for about 1 h. The electrochemically active surface areas (ECSA) was estimated by the equation ECSA = Q_o/q_o, where Q_o is the surface charge obtained from the area under the CV trace for the reduction of metal oxide, and q_o is the charge required for desorption of monolayer of oxygen on the Pd surface (424 μC cm^{-2}).[6]

RESULTS AND DISCUSSION

NP Synthesis and Characterization. One-pot synthesis of monodisperse Pd–Ni alloy NPs was achieved by the co-reduction of $Pd(acac)_2$ and $Ni(acac)_2$ with TBAB in the presence of OA and OAm. Hereafter, we will refer to the alloy NPs prepared from the $Pd(acac)_2/Ni(acac)_2$ mixtures in molar ratios of 1/1 and 1/3 as $Pd_{50}Ni_{50}$ and $Pd_{25}Ni_{75}$ NPs, respectively. Images a and b in Figure 1 show typical TEM images of the prepared Pd–Ni nanoalloys. Regardless of the NP compositions, the measured mean particle diameters were about 5 nm (4.9 ± 0.5 nm). The synthesized NPs had a spherical shape with narrow size distribution. According to the ICP-AES data analyses, the actual compositions of $Pd_{50}Ni_{50}$ and $Pd_{25}Ni_{75}$ NPs were determined to be $Pd_{46}Ni_{54}$ and $Pd_{28}Ni_{72}$, respectively, which were highly consistent with those of the raw solutions. Noticeably, NPs prepared from the $Pd(acac)_2/Ni(acac)_2$ mixture in a molar ratio of 3/1 ($Pd_{75}Ni_{25}$ NPs) were not homogeneous in shape and size compared to $Pd_{50}Ni_{50}$ and $Pd_{25}Ni_{75}$ NPs (Figure S1 in the Supporting Information), implying that a relatively large amount Pd precursor could not induce the formation of monodisperse NPs. In a previous work,

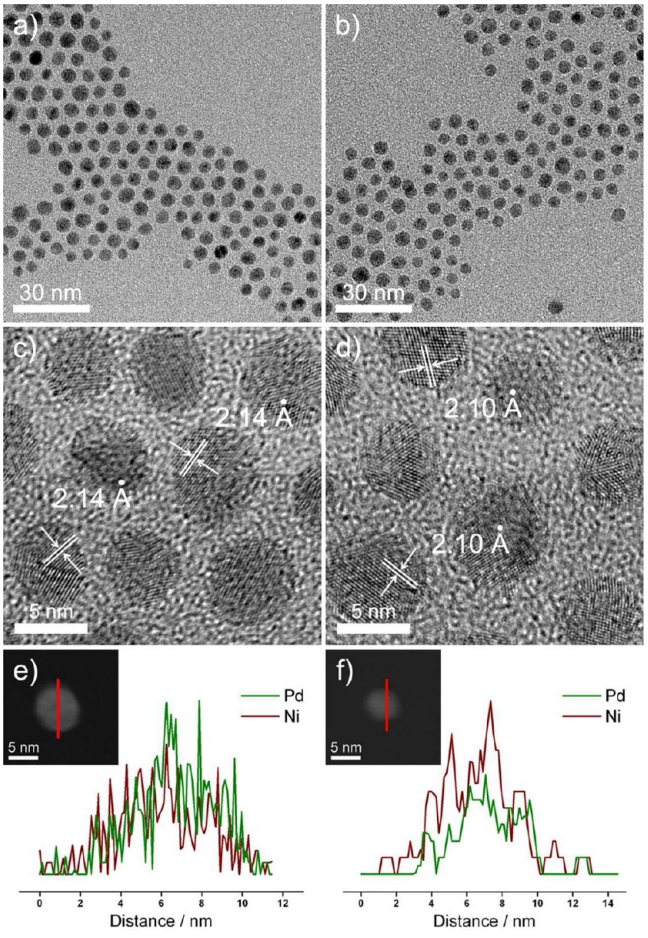

Figure 1. TEM images of (a) $Pd_{50}Ni_{50}$ and (b) $Pd_{25}Ni_{75}$ NPs. HRTEM images of (c) $Pd_{50}Ni_{50}$ and (d) $Pd_{25}Ni_{75}$ NPs. HAADF-STEM images and corresponding compositional line profiles of (e) $Pd_{50}Ni_{50}$ and (f) $Pd_{25}Ni_{75}$ NP.

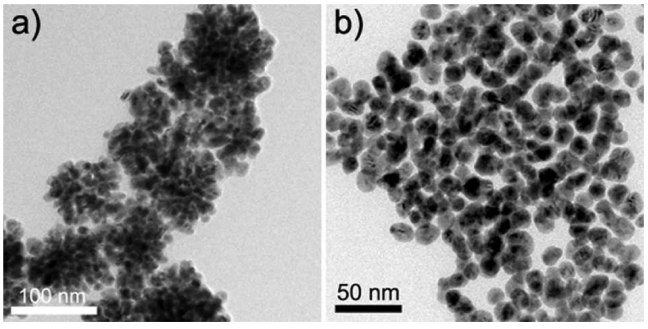

Figure 2. TEM images of NPs prepared without (a) TBAB and (b) OA.

we found that monometallic Pd NPs have low suspension stability at high temperature and alloying them with other metals, such as Cu, can increase the stability of the resultant NPs.[7] The generation of inhomogeneous $Pd_{75}Ni_{25}$ NPs can thus be attributed to the low thermal stability of Pd. In fact, NPs prepared with a reaction mixture containing only $Pd(acac)_2$ as a metal precursor under otherwise identical synthetic conditions had irregular shapes and easily aggregated (see Figure S2 in the Supporting Information). On the basis of the successful production of homogeneous NPs from the $Pd(acac)_2/Ni(acac)_2$ mixtures in molar ratios of 1/1 and 1/3,

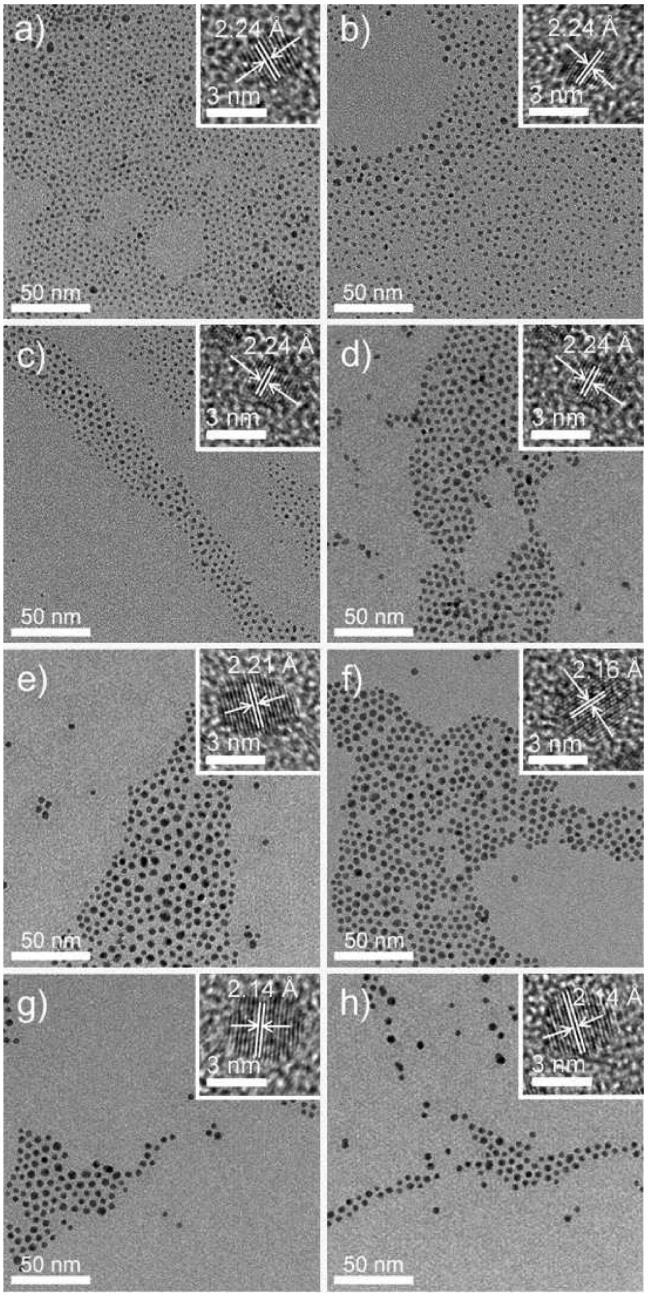

Figure 3. TEM images of $Pd_{50}Ni_{50}$ NPs at (a) 50, (b) 100, (c) 150, (d) 200, (e) 230, (f) 250, (g) 270, and (h) 300 °C. HRTEM images of NPs are shown in each inset.

we can infer that Ni plays a critical role in the synthesis of monodisperse Pd−Ni NPs by increasing the thermal stability of NPs.

To investigate the fine structure of the prepared Pd−Ni NPs, HRTEM characterization was performed. Figures 1c and 1d show HRTEM images of $Pd_{50}Ni_{50}$ and $Pd_{25}Ni_{75}$ NPs, respectively, revealing the well-defined crystalline structures of the NPs. The lattice spacings for $Pd_{50}Ni_{50}$ and $Pd_{25}Ni_{75}$ NPs were measured to be 2.14 and 2.10 Å, respectively, which could be assigned to the *d*-spacings for the (111) planes of Pd−Ni alloys. By using the Pd/Ni ratios determined by ICP-AES and the lattice constants of Pd (a = 3.8898 Å; JCPDS-ICDD 005-0681) and Ni (a = 3.5238 Å; JCPDS-ICDD 004-0850), the *d*-spacings could be calculated from Vegard's law:[15] 2.13 Å for

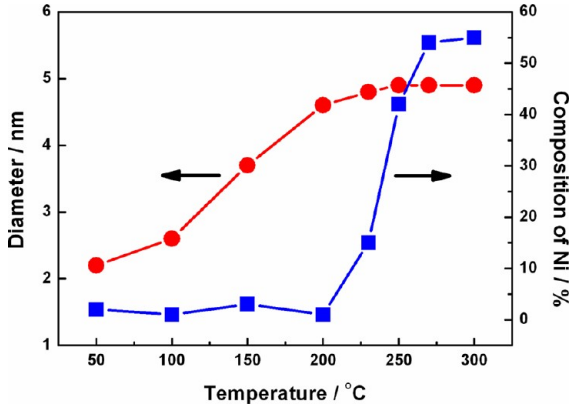

Figure 4. The changes in mean particle diameter and Ni composition of $Pd_{50}Ni_{50}$ NPs at the different reaction temperatures.

Table 1. Compositions, Average Particle Sizes, and *d*-Spacings of $Pd_{50}Ni_{50}$ NPs Prepared at the Different Reaction Temperatures

	50 °C (2 min)	100 °C (5 min)	150 °C (8 min)	200 °C (12 min)
composition	$Pd_{98}Ni_2$	$Pd_{99}Ni_1$	$Pd_{97}Ni_3$	$Pd_{99}Ni_1$
Size (nm)	2.2	2.6	3.7	4.6
d-spacing (Å)	2.24	2.24	2.24	2.24
	230 °C (14 min)	250 °C (15 min)	270 °C (16 min)	300 °C (18 min)
Composition	$Pd_{85}Ni_{15}$	$Pd_{58}Ni_{42}$	$Pd_{46}Ni_{54}$	$Pd_{45}Ni_{55}$
Size (nm)	4.8	4.9	4.9	4.9
d-spacing (Å)	2.21	2.16	2.14	2.14

$Pd_{50}Ni_{50}$ NPs and 2.09 Å for $Pd_{25}Ni_{75}$ NPs, which are in good agreement with the values observed in the HRTEM images. HAADF-STEM-EDS results further verify the alloy nature of the prepared Pd−Ni NPs (Figure 1e, f). The XRD patterns of the Pd−Ni NPs show distinct diffraction peaks from the reflections of the face-centered cubic (fcc) metal (see Figure S3 in the Supporting Information), indicating the crystallinity of the prepared NPs. It is noticeable that the 2θ values of Pd−Ni NPs lie between those of pure Pd and Ni, revealing the formation of single-phase alloy NPs. The surface compositions of the $Pd_{50}Ni_{50}$ and $Pd_{25}Ni_{75}$ NPs were determined to be Pd:Ni = 84:16 and 80:20, respectively, by XPS (see Figure S4 in the Supporting Information), unambiguously indicating the alloy nature of their surfaces, as evidenced by the HRTEM, HAADF-STEM-EDS, and XRD measurements. It is noteworthy that surface compositions of the prepared Pd−Ni alloy NPs significantly deviated from those obtained by ICP-AES: the NPs had a Pd-enriched surface. The difference in composition between the surface and bulk of the Pd−Ni alloy NPs can be attributed to their formation mechanism. This will be discussed later (vide infra).

It has been known that the use of amine-borane complexes as reductants is very effective for the preparation of monodisperse NPs. For example, Sun and co-workers reported that uniform Pd NPs could be synthesized by tributylamine-borane complex.[16] Stucky et al. also reported the production of monodisperse metallic NPs with TBAB.[17] In fact, flowerlike NPs with a porous structure, which were composed of small nanoparticular segments, were generated without TBAB under otherwise identical synthetic conditions (Figure 2a). Because OAm is a mild reductant, a multi-nucleation process was

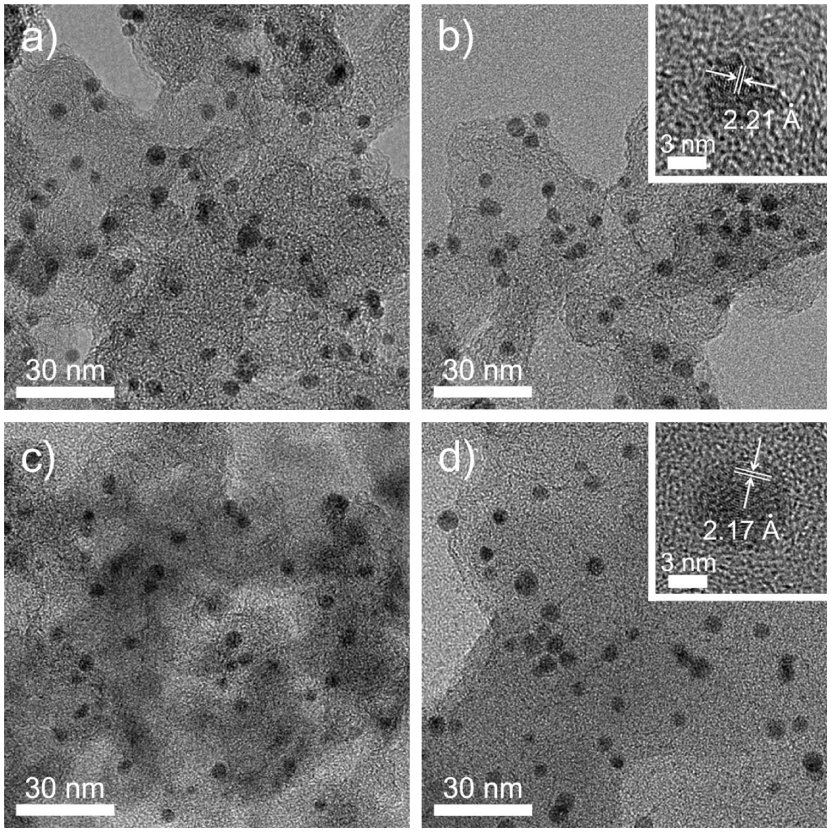

Figure 5. TEM images of carbon-supported (a) $Pd_{50}Ni_{50}$ and (c) $Pd_{25}Ni_{75}$ NPs. TEM and HRTEM images of (b) $Pd_{86}Ni_{14}$/C and (d) $Pd_{59}Ni_{41}$/C.

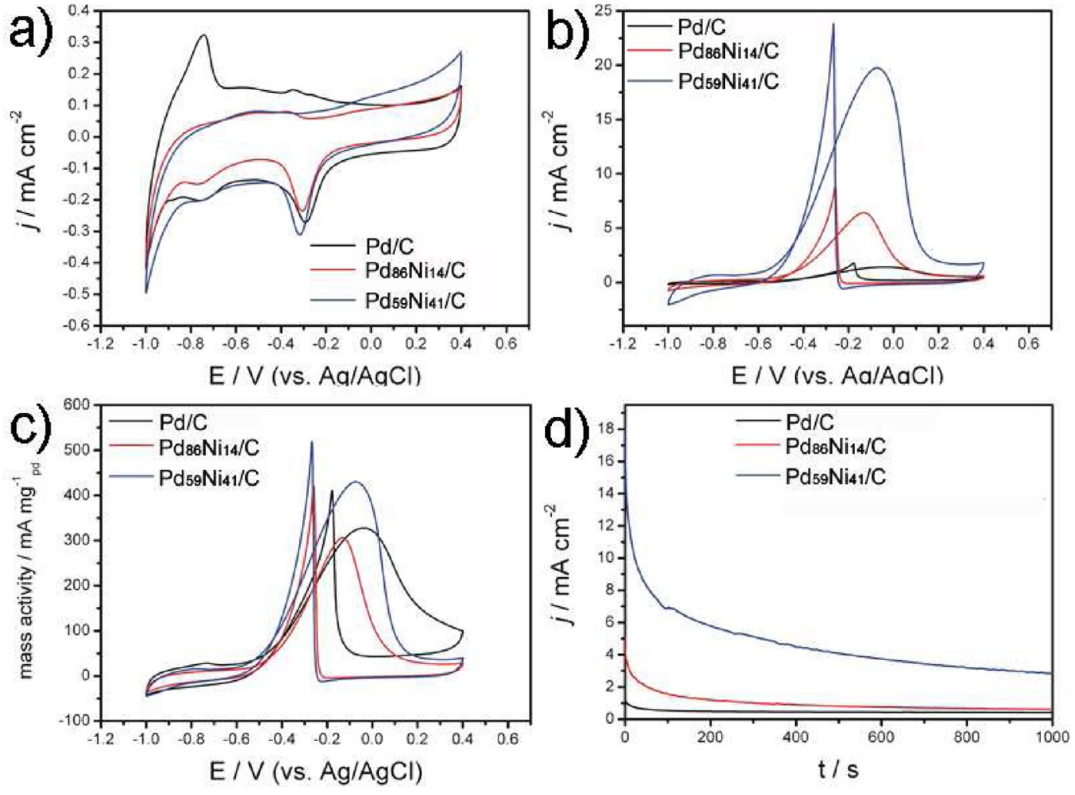

Figure 6. CV curves of $Pd_{86}Ni_{14}$/C, $Pd_{59}Ni_{41}$/C, and commercial Pd/C catalysts in (a) 0.1 M KOH and (b) 0.1 M KOH + 0.5 M ethanol. Scan rate: 50 mV s^{-1}. Current values were normalized to the ECSA. (c) Mass activities of catalysts in 0.1 M KOH + 0.5 M ethanol. (d) CA curves of $Pd_{86}Ni_{14}$/C, $Pd_{59}Ni_{41}$/C, and commercial Pd/C catalysts in 0.1 M KOH + 0.5 M ethanol at −0.2 V vs. Ag/AgCl.

dx.doi.org/10.1021/am300923s | ACS Appl. Mater. Interfaces 2012, 4, 4208−4214

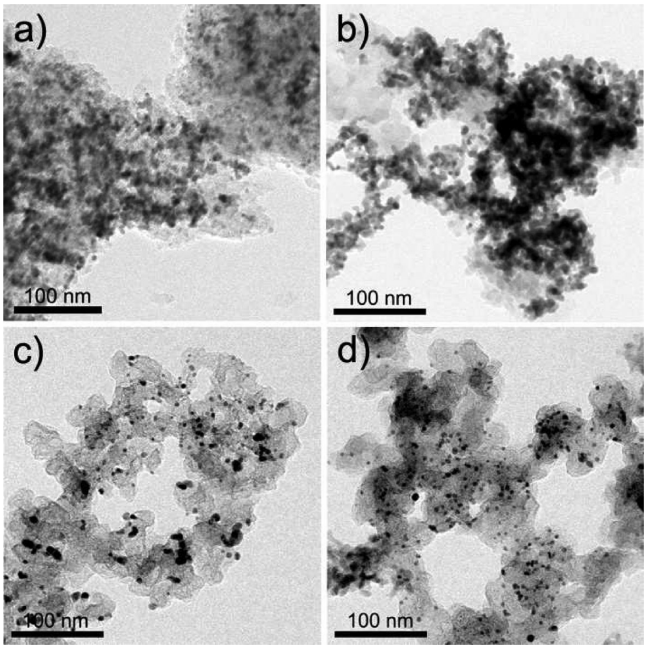

Figure 7. TEM images of commercial Pd/C (a) before and (b) after the electrochemical tests. TEM images of (c) $Pd_{86}Ni_{14}$/C and (d) $Pd_{59}Ni_{41}$/C catalysts after the electrochemical tests.

induced by OAm, and consequently unevenly sized and shaped NPs were developed where only OAm was used as a reducing agent.[16] Therefore, thanks to the use of TBAB as an effective reductant, monodisperse 5 nm NPs could be prepared under our experimental conditions. Furthermore, employing both OA and OAm facilitated the formation of monodisperse Pd–Ni NPs. Without OA, nonuniform NPs with a larger particle size (10-15 nm) than those of the $Pd_{50}Ni_{50}$ and $Pd_{25}Ni_{75}$ NPs were obtained (Figure 2b). This demonstrates that the OA/OAm combination serves as an effective stabilizing agent during the growth of NPs. Similar observations were made in previous works on the synthesis of bimetallic NPs.[18−20]

To decipher the formation mechanism of Pd–Ni alloy NPs, temporal changes in the structure and composition of $Pd_{50}Ni_{50}$ NPs were investigated. TEM images of samples obtained at various reaction temperatures are shown in Figure 3, and corresponding changes in mean particle diameter and Ni composition of NPs are summarized in Figure 4. Compositions and structural parameters of NPs are also summarized in Table 1. Figure 3a shows that small NPs with an average size of 2.2 nm formed at the initial stage of the reaction (2 min, 50°C). The lattice spacing of the (111) planes for the initially formed NPs was determined to be 2.24 Å (inset of Figure 3a). In addition, the ICP-AES-determined composition of NPs was $Pd_{98}Ni_2$. The theoretical lattice spacing of the (111) planes for $Pd_{98}Ni_2$ NPs calculated by Vegard's law was 2.24 Å, which is identical to the experimental value. Up to 200°C (12 min), no noticeable change in the composition of NPs was observed, while the mean NP size increased to 4.6 nm (Figure 3b–d, Figure 4, and Table 1). The HRTEM images shown in the insets of Figures 3b-d further demonstrate that the values of lattice spacing are identical between samples. Together with the ICP-AES results, this implies that NPs formed up to 200°C are mostly composed of Pd with a negligible amount of Ni. After 200°C, the Ni composition significantly increased along with a slight increase of NP size. Figure 3e shows TEM image of 4.8 nm Pd–Ni NPs formed at 230°C. The measured lattice spacing of 2.21 Å is the same as the theoretical *d*-spacing of $Pd_{85}Ni_{15}$ (ICP-AES-determined composition of NPs). Beyond 250 °C, the synthesized Pd–Ni NPs were similar in shape and size regardless of the reaction temperatures (Figure 3f–h)

From these experimental results, we can speculate about the likely mechanism for the formation of Pd–Ni alloy NPs. First, small Pd NPs are generated at ~50 °C before the formation of Pd–Ni alloy NPs. This may be due to the higher reduction potential of Pd(II) than that of Ni(II). These Pd NPs can then serve as active seeds in the subsequent growth of NPs. As the reaction temperature increases, the average size of the Pd NPs increases. Above 200 °C, Ni^{2+} ions start to be reduced to Ni atoms on the active sites of the Pd NP surfaces. When a similar reaction was performed with a solution containing only $Ni(acac)_2$ as a metal precursor, Ni^{2+} ions could not be reduced until the reaction temperature reached to 260 °C, indicating that the reduction of Ni^{2+} ion is facilitated by the preformed Pd NPs through the autocatalytic growth mechanism.[21,22] The deposited surface Ni atoms are then mixed with Pd atoms through the interdiffusion process because of thermal energy, eventually resulting in the formation of homogeneous Pd–Ni alloy NPs. One might expect that the sequential nucleation of Pd and Ni precursors yields core-shell Pd@Ni NPs. In fact, co-reduction of metal precursors with different reduction potentials frequently produced core-shell NPs under mild reducing environment, such as low temperature and the use of mild reductant, where the metal with higher reduction potential composed the core.[23,24] However, we could not identify the formation of Pd@Ni NPs under our experimental conditions, implying that high thermal energy associated with the high reaction temperature enforced the aforementioned interdiffusion of Pd and Ni, thereby generating the Pd–Ni NPs with homogenous alloy structure. This type of growth process has been proposed in previous works on the fabrication of homogeneous bimetallic alloy NPs.[21,22,25,26] Furthermore, higher cohesive energy, higher surface energy, and smaller atomic size of Ni compared with Pd could result in the enhancement of the diffusion of Ni atoms from the surface to the inner part of NPs.[27] As such, Pd–Ni alloy NPs with a Pd-enriched surface were produced, as revealed by XPS measurements. To further confirm the suggested mechanism for the formation of Pd–Ni alloy NPs, we tested the possibility of the generation of Pd–Ni alloy NPs by using pre-synthesized Pd NPs as seeds for the nucleation of Ni in a decoupled two-step synthesis. In fact, injection of $Ni(acac)_2$ into a solution containing pre-synthesized Pd NPs at 270 °C produced Pd–Ni alloy NPs, though the size and shape of NPs were very inhomogeneous compared to those of NPs prepared by the one-pot synthesis method and they were readily aggregated (see Figure S5 in the Supporting Information). These findings verify that the Pd–Ni alloy NPs form via the proposed sequential nucleation–interdiffusion mechanism and the simultaneous reduction of both metal precursors by the present one-pot protocol is the key to the formation of monodisperse NPs.

Electrocatalysis. We investigated the catalytic activity of the prepared Pd–Ni alloy NPs toward ethanol electro-oxidation and the results were compared with those of a commercial Pd/C catalyst, where spherical Pd NPs with an average size of 4.7 ± 0.9 nm were deposited on activated carbon. For electrochemical tests, the as-prepared 5 nm Pd–Ni NPs were loaded onto Ketjen Black carbon. Figures 5a and 5c

show TEM images of $Pd_{50}Ni_{50}$/C and $Pd_{25}Ni_{75}$/C catalysts, respectively. As shown in the images, Pd−Ni NPs are evenly dispersed on carbon supports and retain their original shape and size. Since surfactant molecules, such as OA/OAm, are bound to NP surfaces and can thus block the catalytically active sites of NPs, the removal of surfactants is an important step in the preparation of NP catalysts.[28,29] Among various treatment methods, acetic acid washing is known as a facile and effective way to eliminate residual organic surfactants and can improve the activity of catalysts.[7,18,19] Images b and d in Figure 5 show TEM images of $Pd_{50}Ni_{50}$/C and $Pd_{25}Ni_{75}$/C catalysts after acetic acid washing. Interestingly, from ICP-AES analyses, the compositions of $Pd_{50}Ni_{50}$/C and $Pd_{25}Ni_{75}$/C were changed to $Pd_{86}Ni_{14}$/C and $Pd_{59}Ni_{41}$/C, respectively. This can be ascribed to the selective dissolution of the Ni component from the Pd−Ni alloy NPs during the acid treatment process. It has been reported that acid treatment for noble-non-noble metal alloy NPs generated dealloyed structures owing to the selective dissolution of less noble elements from alloy NPs, and these chemically dealloyed NPs often exhibit improved catalytic properties compared to normal alloy NPs.[16,30] The lattice spacings of 2.21 and 2.17 Å, respectively, for $Pd_{86}Ni_{14}$/C and $Pd_{59}Ni_{41}$/C determined by HRTEM measurements (insets of images b and d in Figure 5) are highly correlated with those calculated using Vegard's law (2.21 Å for $Pd_{86}Ni_{14}$ and 2.15 Å for $Pd_{59}Ni_{41}$).

Figure 6a shows the CV curves of $Pd_{86}Ni_{14}$/C, $Pd_{59}Ni_{41}$/C, and commercial Pd/C in a 0.1 M KOH solution displaying typical redox peaks associated with the oxidation/reduction of Pd. Figure 6b depicts the specific current densities of $Pd_{86}Ni_{14}$/C, $Pd_{59}Ni_{41}$/C, and Pd/C recorded in 0.1 M KOH solution containing 0.5 M ethanol, respectively. The current values were normalized to ECSA. Current densities of $Pd_{86}Ni_{14}$/C and $Pd_{59}Ni_{41}$/C are 6.53 and 19.83 mA cm^{-2}, respectively, which are 4.2 and 12.7 times higher than that of Pd/C (1.56 mA cm^{-2}), respectively. Furthermore, the onset potentials of the $Pd_{86}Ni_{14}$/C and $Pd_{59}Ni_{41}$/C catalysts negatively shift compared to Pd/C: the onset potential values of $Pd_{86}Ni_{14}$/C, $Pd_{59}Ni_{41}$/C, and Pd/C are −0.42, −0.56, and −0.36 V vs. Ag/AgCl, respectively. Mass activity of $Pd_{59}Ni_{41}$/C is also higher than those of other catalysts (Figure 6c). Taken together, these experimental results indicate that the Pd−Ni NPs/C catalysts have highly enhanced catalytic activity for ethanol electrooxidation compared to Pd/C, and $Pd_{59}Ni_{41}$/C shows better electrocatalytic performance than $Pd_{86}Ni_{14}$/C. Because a smaller amount of Pd is required to produce $Pd_{59}Ni_{41}$/C than $Pd_{86}Ni_{14}$/C, $Pd_{59}Ni_{41}$/C can be an efficient and economical catalyst for fuel cell applications.

The long-term electrochemical stability of Pd−Ni NPs/C catalysts for ethanol oxidation was investigated by chronoamperometry (CA) experiments. Figure 6d shows the CA curves of $Pd_{86}Ni_{14}$/C, $Pd_{59}Ni_{41}$/C, and Pd/C at -0.2 V vs. Ag/AgCl. The current decays of Pd−Ni NPs/C are slower than that of Pd/C. In particular, the current decay of $Pd_{59}Ni_{41}$/C is much slower than that of $Pd_{86}Ni_{14}$/C, indicating that the $Pd_{59}Ni_{41}$/C catalysts have better electrochemical stability and electrocatalytic activity than the $Pd_{86}Ni_{14}$/C catalyst. To further confirm the electrochemical stability of Pd−Ni NPs/C catalysts, their TEM images were obtained after electrochemical tests (Figure 7). Although extended agglomeration was observed for Pd/C after the test, there was no considerable change in the Pd−Ni NPs/C catalysts.

CONCLUSIONS

Facile and reproducible one-pot synthesis of monodisperse 5 nm Pd−Ni nanoalloys was presented. Pd−Ni alloy NPs were prepared by the reduction of $Pd(acac)_2$/$Ni(acac)_2$ mixtures in molar ratios of 1/1 and 1/3 using TBAB, OA, and OAm. Employing TBAB as an effective reductant and OA/OAm combination as an effective stabilizing agent facilitated the formation of monodisperse Pd−Ni NPs. Experimental results identified that the Pd−Ni alloy NPs form through the sequential nucleation-interdiffusion mechanism and the simultaneous reduction of both metal precursors by the one-pot synthesis protocol is the key to the formation of homogeneous NPs. The Pd−Ni NPs were well dispersed on carbon supports and chemically dealloyed after acetic acid washing. The Pd−Ni NP catalysts exhibited significantly improved electrocatalytic activity and stability for ethanol oxidation compared to a commercial Pd/C catalyst. We expect that Pd−Ni NPs will be useful as efficient and economical anode catalysts in the development of DEFCs.

ASSOCIATED CONTENT

Supporting Information

Additional experimental data (Figure S1−5). This material is available free of charge via the Internet at http://pubs.acs.org.

AUTHOR INFORMATION

Corresponding Author

*E-mail: sangwoohan@kaist.ac.kr.

Author Contributions

†These authors contributed equally to this work.

Notes

The authors declare no competing financial interest.

ACKNOWLEDGMENTS

This work was supported by Basic Science Research Programs (2010-0029149), EPB Center (2008-0062042), the PRC Program (2009-0082813), and Future-based Technology Development Program (Nano Fields) (2009-0082640) through the National Research Foundation (NRF) funded by the Korean government (MEST).

REFERENCES

(1) Lamy, C.; Lima, A.; LeRhun, V.; Delime, F.; Coutanceau, C.; Léger, J.-M. *J. Power Sources* **2002**, *105*, 283.
(2) Parrondo, J.; Santhanam, R.; Mijangos, F.; Rambabu, B. *Int. J. Electrochem. Sci.* **2010**, *5*, 1342.
(3) Mazumder, V.; Lee, Y.; Sun, S. *Adv. Funct. Mater.* **2010**, *20*, 1224.
(4) Bianchini, C.; Shen, P. K. *Chem. Rev.* **2009**, *109*, 4183.
(5) Hong, J. W.; Kim, D.; Lee, Y. W.; Kim, M.; Kang, S. W.; Han, S. W. *Angew. Chem. Int. Ed.* **2011**, *50*, 8876.
(6) Lee, Y. W.; Kim, M.; Kang, S. W.; Han, S. W. *Angew. Chem., Int. Ed.* **2011**, *50*, 3466.
(7) Park, K.-H.; Lee, Y. W.; Kang, S. W.; Han, S. W. *Chem. Asian J.* **2011**, *6*, 1515.
(8) Jiang, H.-L.; Xu, Q. *J. Mater. Chem.* **2011**, *21*, 13705.
(9) Du, C.; Chen, M.; Wang, W.; Yin, G.; Shi, P. *Electrochem. Commun.* **2010**, *12*, 843.
(10) Zhang, Z.; Nenoff, T. M.; Leung, K.; Ferreira, S. R.; Huang, J. Y.; Berry, D. T.; Provencio, P. P.; Stumpf, R. *J. Phys. Chem. C* **2010**, *114*, 14309.
(11) Zhao, J.; Sarkar, A.; Manthiram, A. *Electrochim. Acta* **2010**, *55*, 1756.
(12) Zhao, Y.; Yang, X.; Tian, J.; Wang, F.; Zhan, L. *Int. J. Hydrogen Energy* **2010**, *35*, 3249.

(13) Gao, Y.; Wang, G.; Wu, B.; Deng, C.; Gao, Y. *J. Appl. Electrochem.* **2011**, *41*, 1.
(14) Singh, S. K.; Iizuka, Y.; Xu, Q. *Int. J. Hydrogen Energy* **2011**, *36*, 11794.
(15) Kang, S. W.; Lee, Y. W.; Kim, M.; Hong, J. W.; Han, S. W. *Chem. Asian J.* **2011**, *6*, 909.
(16) Mazumder, V.; Sun, S. *J. Am. Chem. Soc.* **2009**, *131*, 4588.
(17) Zheng, N.; Fan, J.; Stucky, G. D. *J. Am. Chem. Soc.* **2006**, *128*, 6550.
(18) Choi, S.-I.; Choi, R.; Han, S. W.; Park, J. T. *Chem. Commun.* **2010**, *46*, 4950.
(19) Choi, S.-I.; Choi, R.; Han, S. W.; Park, J. T. *Chem. Eur. J* **2011**, *17*, 12280.
(20) Abdelsayed, V.; Aljarash, A.; El-Shall, M. S.; Al Othman, Z. A.; Alghamdi, A. H. *Chem. Mater.* **2009**, *21*, 2825.
(21) Snyder, J.; McCue, I.; Livi, K.; Erlebacher, J. *J. Am. Chem. Soc.* **2012**, *134*, 8633.
(22) Carpenter, M. K.; Moylan, T. E.; Kukreja, R. S.; Atwan, M. H.; Tessema, M. M. *J. Am. Chem. Soc.* **2012**, *134*, 8535.
(23) Yan, J.-M.; Zhang, X.-B.; Akita, T.; Haruta, M.; Xu, Q. *J. Am. Chem. Soc.* **2010**, *132*, 5326.
(24) Lee, Y. W.; Kim, M.; Kim, Z. H.; Han, S. W. *J. Am. Chem. Soc.* **2009**, *131*, 17036.
(25) Chen, W.; Yu, R.; Li, L.; Wang, A.; Peng, Q.; Li, Y. *Angew. Chem., Int. Ed.* **2010**, *49*, 2917.
(26) Shibata, T.; Bunker, B. A.; Zhang, Z.; Meisel, D.; Vardeman, C. F., II; Gezelter, J. D. *J. Am. Chem. Soc.* **2002**, *124*, 11989.
(27) Ferrando, R.; Jellinek, J.; Johnston, R. L. *Chem. Rev.* **2008**, *108*, 845.
(28) Bu, W.; Chen, Z.; Chen, F.; Shi, J. *J. Phys. Chem. C* **2009**, *113*, 12176.
(29) Liu, Y.; Wang, C.; Wei, Y.; Zhu, L.; Li, D.; Jiang, J. S.; Markovic, N. M.; Stamenkovic, V. R.; Sun, S. *Nano Lett.* **2011**, *11*, 1614.
(30) Dutta, I.; Carpenter, M. K.; Balogh, M. P.; Ziegelbauer, J. M.; Moylan, T. E.; Atwan, M. H.; Irish, N. P. *J. Phys. Chem. C* **2010**, *114*, 16309.